Progress In Electromagnetics Research B, Vol. 79, 83–101, 2017

An Experimental 13.56 MHz Radio Frequency Heating System for Efficient Thermal Pretreatment of Wastewater Sludge

Md. S. Ferdous, Ehssan H. Koupaie, Cigdem Eskicioglu, and Thomas Johnson*

Abstract—This paper describes the design of an experimental radio frequency (RF) heating system for efficiently heating waste activated sludge (WAS), a byproduct of wastewater treatment plants. Thermal pretreatment is used to increase the bio-gas yield from subsequent anaerobic processes which use WAS. The RF heating system operates at a frequency of 13.56 MHz and the frequency was selected based on a study of the electrical properties of WAS. RF heating has advantages over microwave heating including access to very efficient RF generators, and RF applicators can be designed to provide uniform heating through large load volumes, overcoming limitations of microwave heating which has a shallow penetration depth in the load. Experimental results for the RF heating system show a dc to RF power conversion efficiency of 85% and a power transfer efficiency from the amplifier to load of more than 86% over a temperature range from 20°C to 120°C.

1. INTRODUCTION

The disposal of wastewater sludge is a costly and difficult environmental problem [1]. The sludge is principally organic matter which is generated after treating wastewater, although increasingly the sludge is being contaminated with other pollutants such as heavy metals and pharmaceutical products. The environmental challenges associated with the disposal of wastewater sludge has led to the investigation of different methods to reduce the volume of sludge after treatment processes, as well as efficient methods to process sludge which re-capture energy from bio-gas generated from decomposition processes [2]. One method that is promising in terms of re-capture of energy is anaerobic digestion [3]. In anaerobic digesters, waste activated sludge (WAS) is placed in an oxygen free environment and anaerobic microorganisms convert organic material into bio-gas through a process called methanogenesis.

An important factor that significantly affects the overall energy efficiency of the anaerobic process is the bio-availability of organic material solubilized in the sludge. Large organic masses called floc, comprised of microbial cells and biopolymers, are typically present in untreated sludge and must first be broken down in smaller organic compounds. Therefore, pre-treatment processes are often used to process sludge before anaerobic digestion. The pre-treatment process breaks down floc to increase the availability of intracellular organic material that is solubilized in the liquid. Different pre-treatment methods can be used including chemical [4], biological [5–7], mechanical [8, 9], thermal [4, 8, 10–13] and non-thermal pulse powered processes [14–16]. Of these methods, thermal pre-treatment processes have been shown to be highly effective, and the design of efficient heating methods to pre-treatment wastewater sludge has motivated this research work.

Received 14 September 2017, Accepted 4 November 2017, Scheduled 13 November 2017
* Corresponding author: Thomas Johnson (thomas.johnson@ubc.ca).
The authors are with the School of Engineering, University of British Columbia, Kelowna, BC, Canada.

1.1. Thermal Pretreatment Methods

In the literature, thermal pretreatment of WAS has been primarily confined to two methods: conventional heating and microwave heating [17–21]. In conventional heating, a source heats the sludge through thermal conduction and thermal convection processes. On the other hand, microwave heating is an electromagnetic heating method and the heating mechanism in the material is associated with the dielectric relaxation of water molecules in a time varying electromagnetic field. Microwave heating is typically implemented at a frequency of 2.45 GHz, although 915 MHz is also used.

Unlike conventional heating, microwave heating is volumetric and heat is generated throughout the load volume by the interaction between the electric field and the material. The disadvantage of microwave heating is that penetration depth is limited and power absorption is highest on exposed surfaces making it difficult to obtain uniform heating through a thick load [22]. The limitations of microwave heating, especially considering scaling to large load volumes, provokes the question: are there other heating frequencies that may be more optimal for thermal pretreatment of WAS?

1.2. Radio Frequency Thermal Pretreatment

In this paper, we present a summary of the electrical characteristics of WAS measured over a large frequency range and conclude that efficient and uniform heating can be obtained at a much lower frequency of 13.56 MHz compared to microwave heating. At 13.56 MHz, the heating mechanism is fundamentally different compared to microwave heating where an ionic conduction current flows through the load rather than dielectric relaxation mechanisms which are dominant at microwave frequencies. WAS has significant conductivity attributed to electrolytes in the material. After considering a range of factors including heating uniformity, the efficiency of high power radio frequency (RF) sources, and the frequency bands available for RF heating, a frequency of 13.56 MHz was selected.

An experimental system was designed to heat samples of WAS and validate the proposed heating frequency at 13.56 MHz. The physical geometry of the applicator was optimized to provide an intrinsic 50 Ω impedance match to the RF source, a 1 kW class E power amplifier. Excellent matching was obtained and the power efficiency of the amplifier was 85%, significantly more efficient than typical magnetron power sources used in microwave heating systems that have efficiencies in the range of 50–60% [23]. The RF heating system has also been used extensively for evaluating the thermal pretreatment of WAS in terms of bio-gas yield for anaerobic digester applications and the interested reader is referred to a separate paper for details [24]. In the following sections, the design methodology and the verification of the RF heating system with a controlled loads (salt water) and WAS loads are described.

2. MATERIALS AND METHODS

If an electromagnetic heating system is to be designed for pre-treating waste-water sludge, it is very important to determine an appropriate frequency for efficient heating. Factors which determine the selection of a heating frequency include the dielectric properties of the material, the power efficiency of the generator, the volume of the load, the temperature profile through the load, and regulatory limitations that restrict heating to specific frequency bands. A consideration of all these factors was made in this work which led to the selection of a heating frequency of 13.56 MHz. The rationale for selecting this frequency is described next.

2.1. Selecting a Heating Frequency for Wastewater Sludge

The amount of power absorbed by a material when exposed to a time varying electric field depends on two electrical properties: conductivity (σ) and permittivity (ϵ). Conductivity is associated with the movement of free charge in a material. When free charge moves in an electric field, it creates ohmic heating resulting from the flow of a conduction current.

Permittivity is a dielectric property associated with bound charge in the material. For the analysis of dielectric heating in a time-harmonic (sinusoidal) electric field, permittivity is complex and expressed as $\epsilon = \epsilon' - j\epsilon''$. Permittivity can also be expressed in a normalised form called the dielectric constant (ϵ_r) where $\epsilon_r = \epsilon/\epsilon_0$ and ϵ_o is the permittivity of free space. The real part (ϵ'_r) is associated with a

non-dissipative displacement current in the dielectric material and the imaginary part (ϵ_r'') is associated with dissipative losses in the dielectric. The dissipative losses are created by dielectric relaxation of polarisation charge in the material.

The dielectric losses can be combined with ohmic power losses to determine how much power is absorbed in a material per unit volume. The power density, p, absorbed by a material in a time varying sinusoidal electric field with a rms amplitude of E_{rms} is

$$p = (\sigma_{DC} + \omega\,\epsilon_r''(\omega)\,\epsilon_o)E_{rms}^2\,\mathrm{W/m^3}. \tag{1}$$

For the frequency range considered in this paper, conductivity is assumed to be independent of frequency, while permittivity is strongly dependent on frequency. Both conductivity and permittivity are also functions of temperature and the sensitivity of these properties to temperature are important in the design of a matching circuit to efficiently transfer power from the amplifier to the load.

Measurements of the dielectric properties of wastewater sludge (WAS) were previously reported in another publication [25]. The dielectric properties were obtained from impedance measurements made using an open circuit coaxial transmission line which was immersed in the sample. With careful calibration and post-processing, the conductivity and complex permittivity were estimated from impedance measurements. Measurements reported in [25] include samples of WAS with a total solid content ratio of 4.5% at a temperature of 25°C and the data are re-plotted in Fig. 1 for convenience of reference.

The electrical properties shown in Fig. 1 give insight into how permittivity changes as a function of frequency. If Eq. (1) is rewritten as

$$p = \left(\epsilon_r'' + \frac{\sigma}{\omega\epsilon_o}\right)\omega\epsilon_o E_{rms}^2, \tag{2}$$

then the power absorbed as a function of frequency is related to the term $\epsilon_r'' + \sigma/(\omega\epsilon_o)$. This term can be found experimentally by dielectric impedance measurements such as the open circuit transmission line method [26].

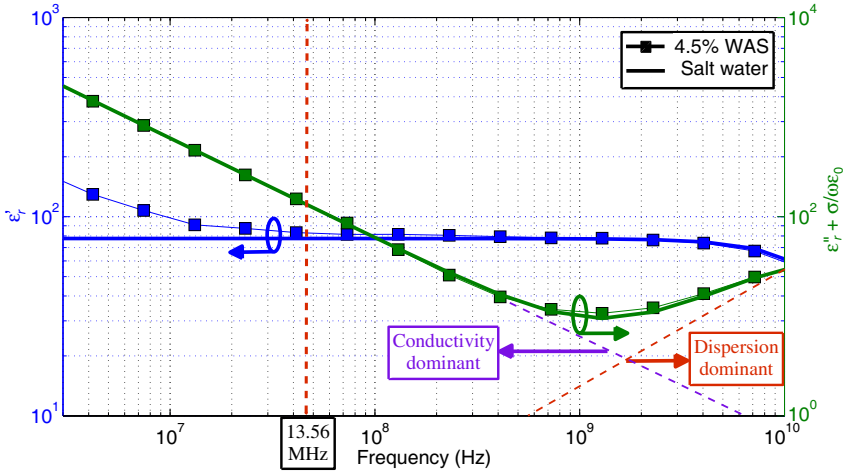

Figure 1. Complex permittivity of 4.5% waste activated sludge. The figure is based on data shown in [25].

If we assume conductivity is constant and independent of frequency, then the measurement data can be separated into a low frequency term ($\sigma/(\omega\epsilon_o)$) which is dominated by the conductivity of the material and a high frequency term which is dominated by the imaginary part (ϵ_r'') of the complex permittivity. The contribution of each term is shown in Fig. 2 and the superposition is equal to the measured characteristic. Based on the measured characteristics of wastewater sludge, we hypothesize that the dielectric characteristics shown in Fig. 2 are dominated by ionic conductivity at low RF frequencies (regions A and B), and by bulk water relaxation at high frequencies in the microwave range (region C).

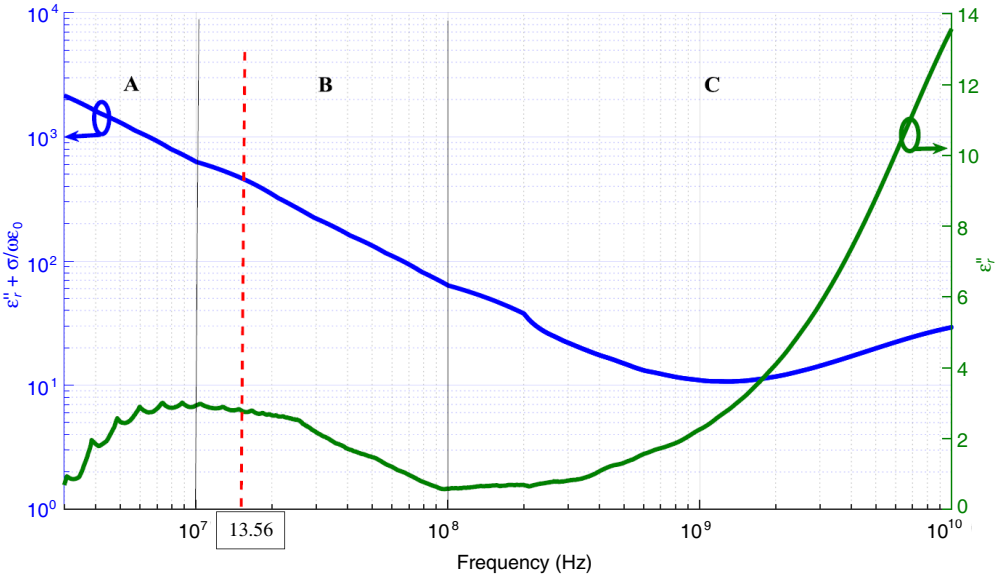

Figure 2. A breakdown of the dissipative material properties of WAS as a function of frequency. The figure is based on data shown in [25].

The application of microwave heating in region C has been reported extensively in the literature, and the objective of this work is to design a RF heating system that operates in region B. RF heating has advantages in terms of the power efficiency of the amplifiers as well as uniform heating through large volumes. The distinction between the two heating methods is that microwave heating uses the dielectric relaxation of water to heat the load, while RF heating uses ohmic heating created by ionic current flow to heat the load.

Since ohmic heating with a conduction current can be extended all the way down to dc, it may be tempting to use dc where very efficient dc power amplifiers could be used to heat the load. However, frequencies that are too low will lead to electrochemical reactions at the interface between the electrodes and the material. Electrochemical reactions can generate dangerous gases, such as hydrogen, as well as build polarisation charge layers on the electrodes [25]. Electrode polarisation is significant up to frequencies around 10 MHz; therefore the low frequency range, identified as region A in Fig. 2, is excluded as a possible heating frequency. This leaves region B as a suitable frequency range for RF heating. Within this frequency range there are allocated frequency bands, called industrial, scientific and medical (ISM) bands, that can be used for RF heating applications. Two ISM bands at 13.56 MHz and 27.12 MHz are shown in region B. RF amplifiers are most efficient at low frequencies and the 13.56 MHz frequency band is selected for this application.

2.2. Equivalent Salt Water Load

Wastewater sludge requires special handling and, as shown in the previous section, the available electrical properties of sludge are limited to measurements made at room temperature (25°C). Therefore an equivalent load with well known electrical characteristics that can be matched to model wastewater sludge is very useful for design and verification. Salts in WAS lead to ionic properties which dominate the low frequency electrical properties of WAS. Using this observation, we constructed an equivalent salt water load which matches the conductivity characteristics of WAS at a temperature of 25°C and then use published models for salt water to predict how electrical properties change over temperature. Standard salt water loads with a molarity adjusted to match WAS low frequency characteristics was an essential part of the design methodology and the heating characteristics of salt water and WAS are well matched as shown later when experimental results are presented.

There are excellent literature references [27] for salt water which give empirical equations for predicting how conductivity and complex permittivity vary with temperature and frequency. The

temperature characteristics of salt water are used in the design to predict how the impedance match between the load and the generator varies over temperature. The complex permittivity of a salt water (SW) solution (ϵ_{sw}) as a function of temperature (T), frequency (f), and salinity (N) is expressed as

$$\epsilon_{SW}(T, f, N) = \epsilon_{\infty,W} + \frac{\epsilon_{o,SW}(T, N) - \epsilon_{\infty,W}}{1 - j2\pi f \tau_{SW}(T, N)} + j\frac{\sigma_{SW}(T, N)}{2\pi f \epsilon_o} \tag{3}$$

In this equation, temperature is in °C, salinity is in moles per litre (also called normality), and $\epsilon_{\infty,W}$ is the high frequency permittivity of water (W) and equal to $4.9\epsilon_o$. The other terms in the equation are dependent on temperature and salinity, and the equations are given in [27]. Using Eq. (3), it was found that a molarity of 0.03315 moles per litre provided a good match with the equivalent dissipation for 4.5% WAS at a frequency of 13.56 MHz.

With reference to Eq. (2), the power dissipation of WAS and salt water are equivalent providing the term $\epsilon_r'' + \frac{\sigma}{\omega\epsilon_o}$ is identical for the two loads. Since salt water does not have a significant ϵ_r'' component at a frequency of 13.56 MHz, the dissipation of the two loads are matched by adjusting the molarity of the salt water to adjust dc conductivity. For equal dissipation, the salt water dc conductivity is 0.342 S/m which is within 1% of the conductivity of WAS (0.34 S/m). A summary of the electrical properties for WAS and the equivalent salt water load are shown in Table 1. The equivalence demonstrates that RF heating at 13.56 MHz is dominated by ohmic heating associated with the conductivity of the load.

In order to gain insight into the temperature sensitivity of the electrical properties of salt water, Eq. (3) is used for a temperature range of 20°C to 120°C which corresponds to the operating temperature range of the RF heating system. The variations of conductivity (σ_{SW}) and relative permittivity ($\epsilon_r' = \mathrm{Re}[\epsilon_{SW}/\epsilon_o]$) as a function of temperature are shown in Fig. 3. The sensitivity of the electrical properties to temperature are important in the design of the RF matching circuit to maximize the

Table 1. Electrical properties of 4.5% WAS and salt water (0.03315 N) for $T = 25$°C and $f = 13.56$ MHz.

Electrical property	WAS	Salt Water
ϵ_r'	92.5	77.7
ϵ_r''	2.8	0
σ_{DC} [S/m]	0.34	0.342
$\epsilon_r'' + \frac{\sigma}{\omega\epsilon_o}$	454	454

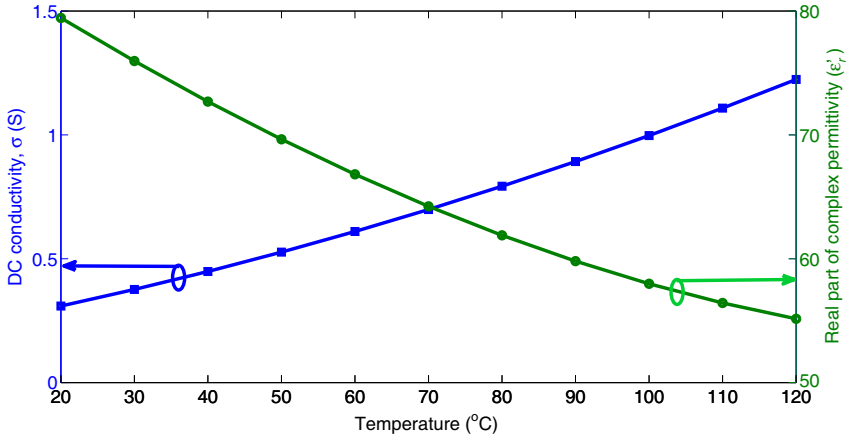

Figure 3. Temperature characteristics of electrical properties of salt water (0.03315 N). DC conductivity (σ) is shown on the left axis and the real part of the relative permittivity (ϵ_r') is shown on the right axis. The data are plotted for a frequency of 13.56 MHz.

transfer of power from the amplifier to the load. As shown, the temperature characteristics are relatively linear over the operating temperature range and the matching circuit design is optimized for the midpoint of the temperature range which is 70°C. Simulation and experimental results presented later confirm that the midpoint is a good choice which maximizes the overall system power efficiency over the entire operating range.

2.3. Physical Design of the RF Heating Applicator

The physical geometry of the heating applicator is very important and affects the heating profile across the load as well as the load impedance. The physical design also needs to be constructed as a pressure vessel to withstand heating under constant volume conditions. Different design concepts were evaluated to balance the electrical and mechanical design constraints and the final design is shown in Fig. 4.

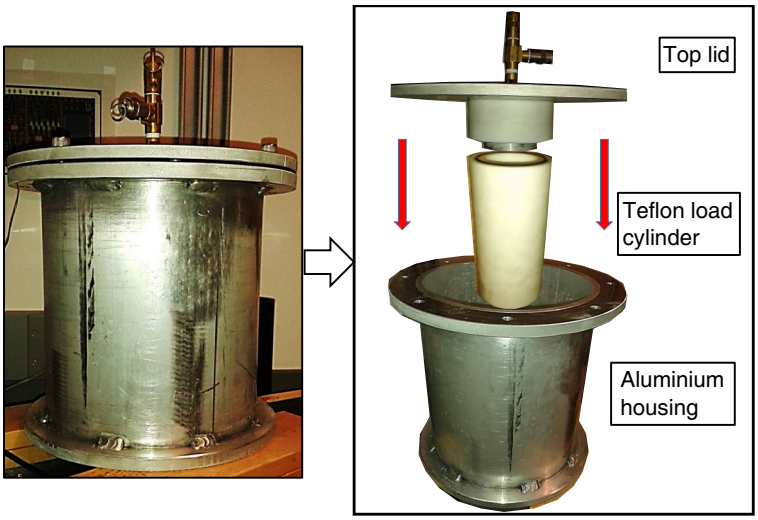

Figure 4. Photograph of the heating applicator. The outside cylinder is constructed from a thick walled aluminum pipe with a top flange welded to secure the removable cylinder cap. Inside the aluminum cylinder is a teflon load cell with electrodes at the top and bottom of the cylinder which make contact with the liquid load. The load cylinder has o-rings to create a pressurized seal. The top electrode includes a safety valve assembly as well as a thermocouple for measuring the internal temperature of the load.

The heating applicator consists of an enclosed aluminum cylinder that meets the mechanical design constraints for pressure as well as provides a complete electrical shield to minimize leakage of RF power. The enclosure is made from aluminum pipe and two flanges are welded to the enclosure. The top flange has holes to bolt the removable top plate of the applicator to the enclosure. The bottom flange is used as a base for the applicator. The aluminum enclosure has an outside diameter of 203 mm, a height of 258 mm, and a wall thickness of 8 mm.

Inside the aluminum housing is an enclosed teflon cylinder that holds the load. Since waste activated sludge is a liquid, the teflon cylinder needs to be completely sealed and o-rings are used between the teflon cap on the cylinder lid and the teflon load vessel. Teflon is used for the load container because it is an insulator, it has very low dielectric losses, it is chemically inert, and it has low thermal conductivity (0.25 W/m/K). The total volume of the teflon load cell is 400 ml and the wall thickness of the teflon pressure vessel is large enough to handle the mechanical stress created by pressure up to temperatures of 120°C. The cylindrical cavity between the inner teflon load cylinder and the outside aluminum cylinder is an air cavity. Thermal insulation could be added to this cavity to reduce thermal conduction losses. Further details on the dimensions of the load cylinder are shown in Fig. 5.

Inside the teflon load cylinder there are two electrodes which create an axial parallel plate capacitor. The parallel plate electrodes create a uniform electric field throughout the load volume which leads to

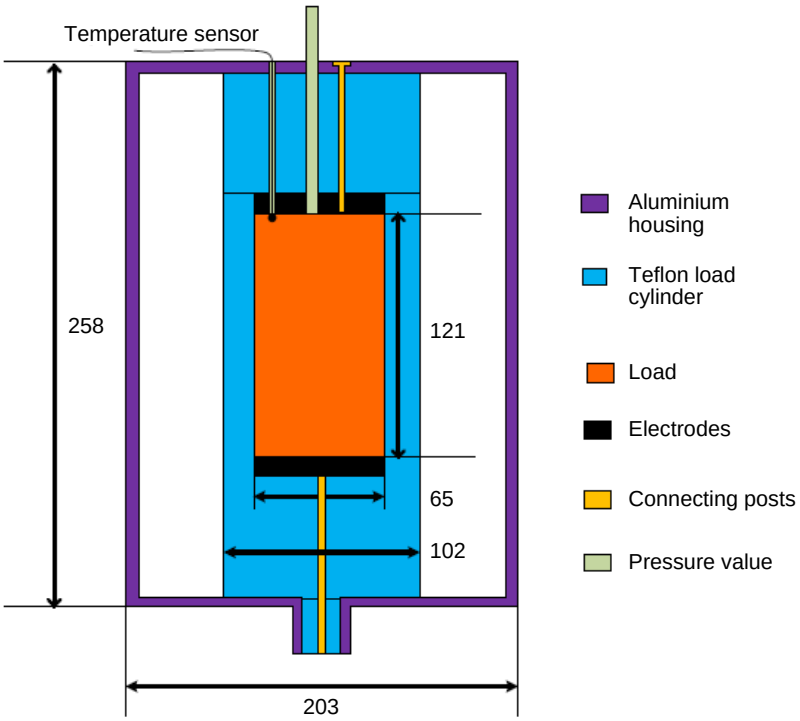

Figure 5. Heating applicator dimensions; units in millimetres.

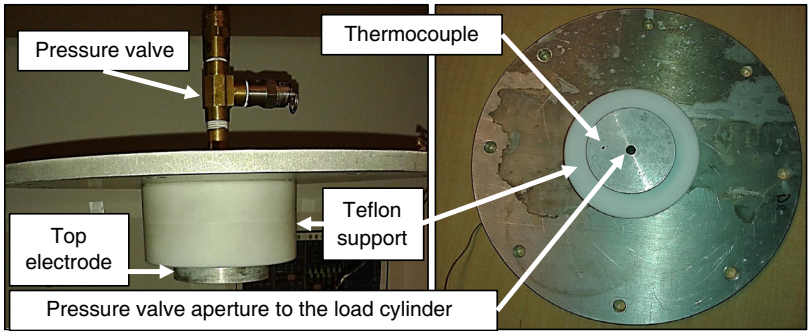

Figure 6. Top electrode assembly for the RF heating applicator. The electrode is connected to ground through the outside coaxial cylinder.

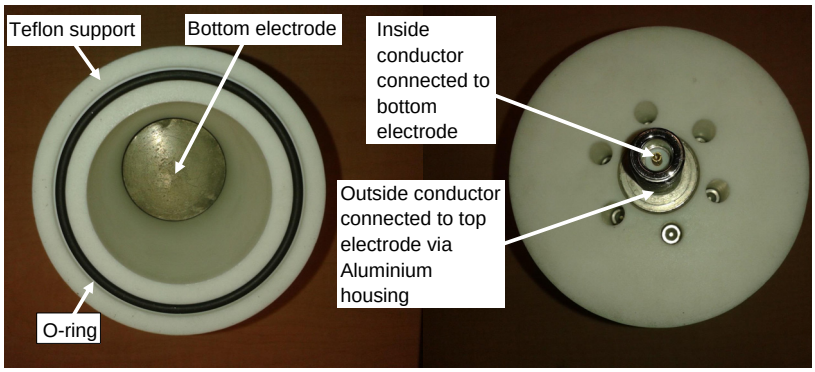

Figure 7. Bottom electrode for the RF heating applicator. The electrode is connected to the centre pin of the coaxial connector.

uniform ohmic heating. The parallel plate structure and the coaxial construction of the teflon load cell and the outside cylinder contribute capacitance to the applicator. The capacitances must be compensated for in the matching circuit to ensure efficient power transfer to the load. An N-type coaxial connector is mounted at the bottom of the enclosure and this is the RF interface to the power amplifier. The centre conductor of the coaxial connector is connected to the bottom electrode and the outside conductor (ground) is connected to the outer aluminum cylinder which is also electrically connected to the top electrode in the cylinder lid.

Photographs of the top and bottom electrodes are shown in Figs. 6 and 7, respectively. The electrodes are made out of 8 mm aluminum plate and electrode corrosion is not expected to be a significant issue because the pH of WAS is approximately neutral (7). The top electrode has a small hole that is fitted with a thermocouple that is sealed. A K-type thermocouple, model GK11M from Test Product International, Inc., is used to measure the temperature of the load.

2.4. Load Impedance Matching Design

An equivalent circuit diagram for the RF heating system is shown in Fig. 8. The RF source is modelled as an ac source with an internal resistance R_s equal to 50 Ω. The load is modelled as two temperature dependent parallel circuit elements, R_{load} and C_{load}. Between the source and load are two reactive L-section circuits; one section models the intrinsic inductance (L_{HA}) and capacitance (C_{HA}) of the physical housing of the applicator, while the other section is a lumped element circuit model for the coaxial cable that interconnects the source and load.

The RF applicator design was optimized in an electromagnetic simulator (COMSOL) [28]. Physical parameters were adjusted to obtain the best impedance match that maximized power transfer efficiency from the source to load over the operating temperature range of the load from 20°C to 120°C. The methodology used to optimize the impedance match of the RF heating applicator is described next.

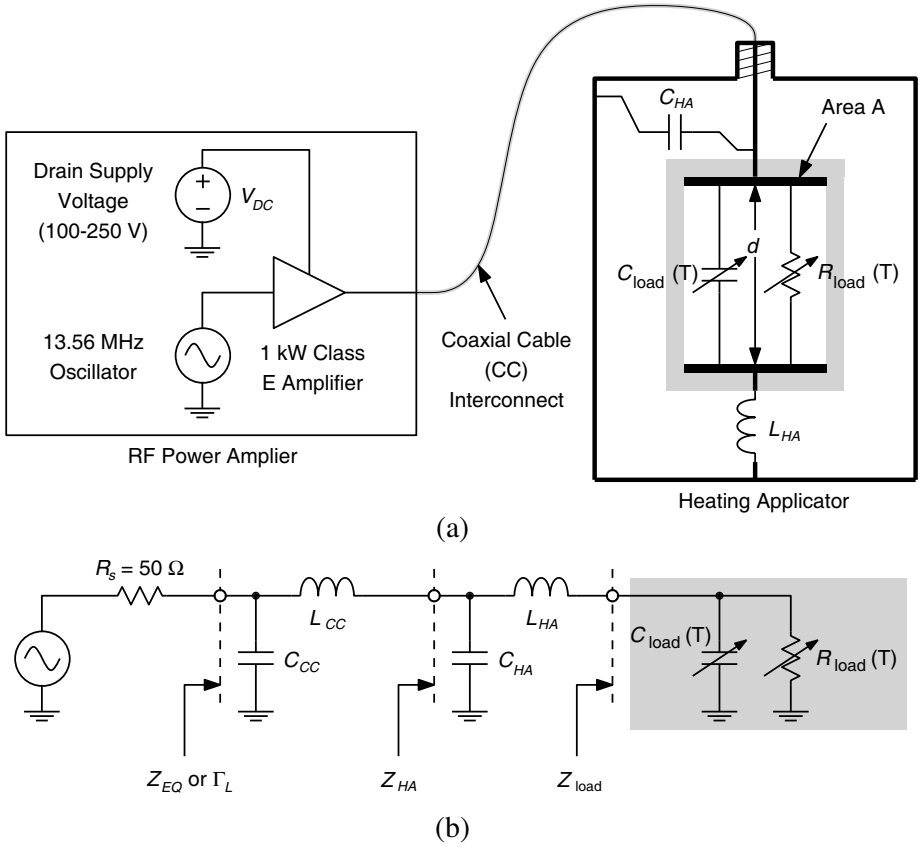

Figure 8. RF heating system models: (a) physical system and (b) equivalent circuit model.

2.5. Power Transfer Efficiency

The power delivered to the load (P_L) is expressed in terms of the load reflection coefficient Γ_L and the maximum available power (P_{av}) which can be delivered by the source (amplifier) to a matched load:

$$P_L = \left(1 - |\Gamma_L|^2\right) P_{av}. \tag{4}$$

The load reflection coefficient is defined at the physical interface between the amplifier and the coaxial cable connecting the amplifier to the load. The corresponding load reflection coefficient is

$$\Gamma_L = \frac{Z_{EQ} - R_s}{Z_{EQ} + R_s} \tag{5}$$

where Z_{EQ} is the equivalent input impedance seen looking into the load, and R_s is the source resistance, $50\,\Omega$ in this design. Using these relations, the power transfer efficiency from the amplifier to the load is

$$\text{Power Transfer Efficiency} = \frac{P_L}{P_{av}} \times 100\%. \tag{6}$$

Equations (4) through (6) are used to calculate simulated and measured power transfer efficiency from the source to the load.

2.5.1. Optimizing Applicator Dimensions for Power Transfer Efficiency

The physical dimensions of the applicator were scaled to set $R_{\text{load}} = 50\,\Omega$ at a temperature of 70°C. A temperature of 70°C corresponds to the mid-point of the operating temperature range for the RF heating system. The salt water load is used for the design, since the analytical models of the electrical properties can be used to predict the overall power transfer efficiency over the entire load operating temperature range. Experimental results shown later compare the heating characteristics of the salt water load with WAS and confirm that the methodology using the equivalent salt water load is a good model for design.

Inside the applicator, the load is sandwiched between two circular electrodes which are at the ends of a teflon cylinder. The structure is modelled as a temperature dependent parallel plate capacitance in shunt with a temperature dependent load resistance. The capacitance and resistance depend on the electrical properties of the load material, the plate area (A) and the distance (d) between the plates:

$$R_{\text{load}}(T) = \frac{1}{\sigma_{DC}(T) + \omega\epsilon_r''\epsilon_o}\left(\frac{A}{d}\right)^{-1} \approx \frac{1}{\sigma_{DC}(T)}\left(\frac{A}{d}\right)^{-1} \tag{7}$$

$$C_{\text{load}}(T) = \epsilon_r'(T)\epsilon_o\left(\frac{A}{d}\right) \tag{8}$$

The approximation in the calculation of R_{load} is made for the salt water load because ϵ_r'' is negligible at a frequency of 13.56 MHz. Using equations for R_{load} and C_{load}, the temperature dependent load impedance, or more conveniently the load admittance, is

$$Y_{\text{load}}(T) = \frac{1}{Z_{\text{load}}} = \frac{1}{R_{\text{load}}(T)} + j2\pi f C_{\text{load}}(T). \tag{9}$$

The temperature dependent electrical properties of the equivalent salt water load are used to determine the dimensions of the teflon load cylinder in the heating applicator. With reference to Fig. 3, at a temperature of 70°C, salt water with a molarity of 0.03315 N has a dc conductivity of 0.73 S/m and a dielectric constant (ϵ_r') of 65. Using Eq. (7), an initial value for $A/d = 0.0274$ is calculated for the condition $R_{\text{load}} = 50\,\Omega$. The required load volume is 400 ml and for this A/d ratio the load cylinder has a diameter of 65 mm and a length of 121 mm.

A complete analysis of the power transfer characteristics of the RF heating system requires electrical models for the coaxial cable and the intrinsic capacitance and inductance of the heating applicator housing. With reference to Fig. 8, the coaxial cable is modeled by a series inductance L_{CC} and a shunt capacitance C_{CC}, while the applicator is modeled by a second equivalent circuit consisting of a series inductance L_{HA} and a shunt capacitance C_{HA}.

A lumped element model for the coaxial cable is easy to derive from the properties of the coaxial cable. The cable is RG-58C/U which has a characteristic impedance (Z_o) of 50 Ω, a nominal capacitance of 101 pF/m and a nominal inductance of 253 nH/m. The length of the cable is 30.5 cm; therefore $C_{CC} = 30.8$ pF and $L_{CC} = 77$ nH. The two element lumped circuit approximation for the coaxial cable is a good approximation at a frequency 13.56 MHz because the wavelength in the coaxial cable is 14.6 m which is much longer than the cable length.

There are no simple closed form solutions for the parasitic capacitance and inductance of the heating applicator housing; therefore, estimated values are derived from COMSOL simulations. The electric field inside the heating applicator can be partitioned into two field regions: 1) the field inside the load volume (V_1) which is related to the energy stored in C_{load}, and 2) a stray field in the remaining volume (V_2) inside the housing associated with the energy stored in C_{HA}. By numerically integrating the electric field energy density (w_e) in the two regions, values of the capacitance can be calculated from the following equations

$$\int_{V_1} w_e dV = \frac{1}{4} C_{\text{load}} V_{pk}^2 \tag{10}$$

and

$$\int_{V_2} w_e dV = \frac{1}{4} C_{HA} V_{pk}^2 \tag{11}$$

where V_{pk} is the peak ac voltage applied across the terminals of the heating applicator. From these equations, numerical estimates of C_{load} and C_{HA} are 15.9 pF and 9.6 pF, respectively. The results show that the capacitance of the load is significantly higher than the stray field capacitance.

A similar method can be used to estimate the parasitic inductance of the applicator except in this case the load has negligible inductance. Therefore, the entire magnetic energy stored inside the applicator volume (V) is used to estimate the inductance of the applicator. The relation between magnetic energy density (w_m) and inductance is

$$\int_{V} w_m dV = \frac{1}{4} L_{HA} I_{pk}^2 \tag{12}$$

where I_{pk} is the peak ac current into the terminals of heating applicator. Using this relation, the numerical estimate of the inductance of the enclosure is 117 nH.

2.5.2. Electric Field across the Load Cylinder

The electromagnetic simulation results can also be used to predict the uniformity of the electric field between the electrodes. The simulator calculates the electric field in a three dimensional model and the field variation in a YZ plane that passes through the center of the load is shown in Fig. 9. The field intensity between the electrodes is plotted as a function of distance from the top electrode. The input power is 1 kW and the electric field is approximately 37 V/cm for the 0.03315 N load. The field is uniform and uniform heating is expected.

2.5.3. Analytic and Simulated Results for Power Transfer Efficiency

Knowing all the circuit parameters in Fig. 8, the analytic equations can be used to predict the temperature dependent impedance characteristics of the load and the overall power transfer efficiency of the system. The analytic results can also be compared with a full electromagnetic simulation of the heating applicator using temperature dependent material properties for the conductivity and permittivity. In COMSOL, the load impedance is measured by calculating the ratio of the phasor voltage over the phasor current at the coaxial connector interface. A comparison of the load impedance using the analytic equations compared with the electromagnetic simulation results is shown in Fig. 10. As shown, the simulated and analytic results are nearly identical and the real part of the load impedance R_{load} is close to 50 Ω at 70°C.

Using the load impedance characteristics as a function of temperature, the circuit model in Fig. 8 can be used to calculate the power transfer efficiency of the RF heating system. The results are shown in Fig. 11. The power transfer efficiency ranges from 85% at 20°C to 93% at 120°C and efficiency

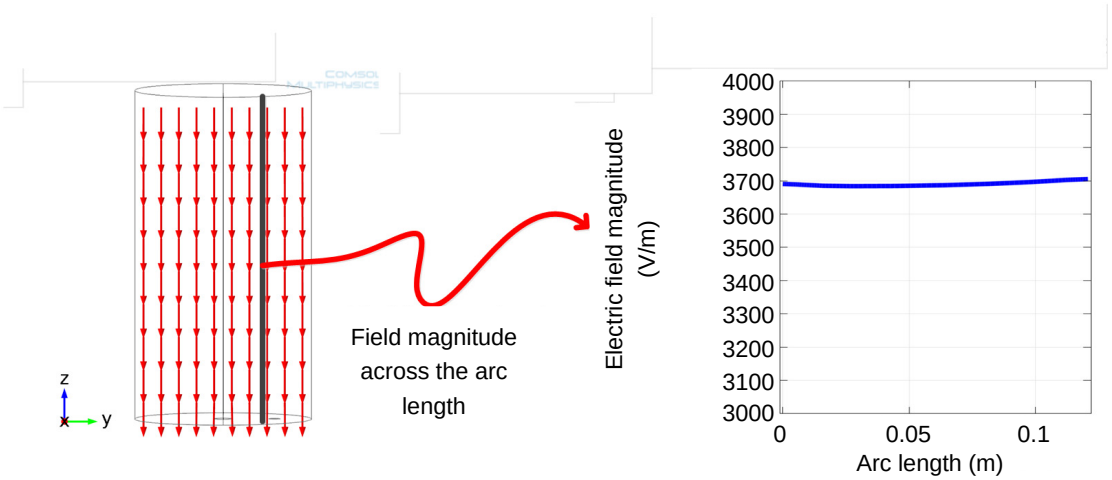

Figure 9. Simulated results for the electric field intensity between the plates. The field is uniform throughout the load volume. The arc length in the right hand figure is equal to 0.121 m, the separation between the electrodes.

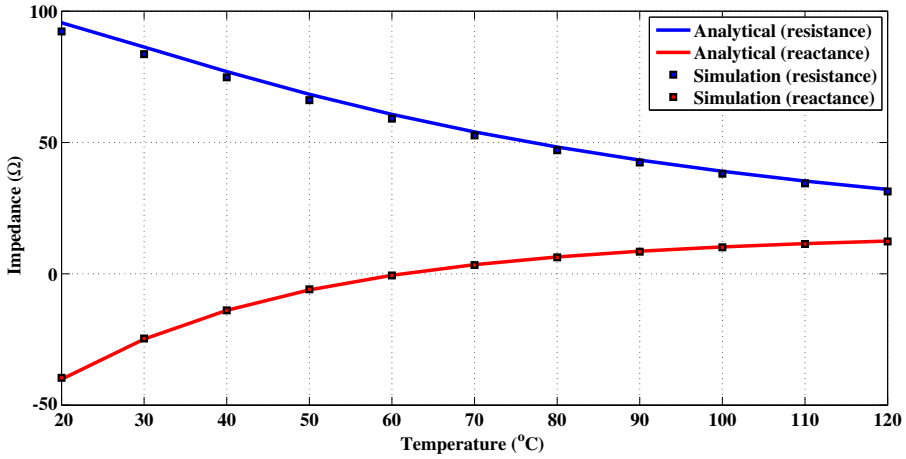

Figure 10. Predicted impedance characteristics versus temperature for a 0.03315 N salt water load.

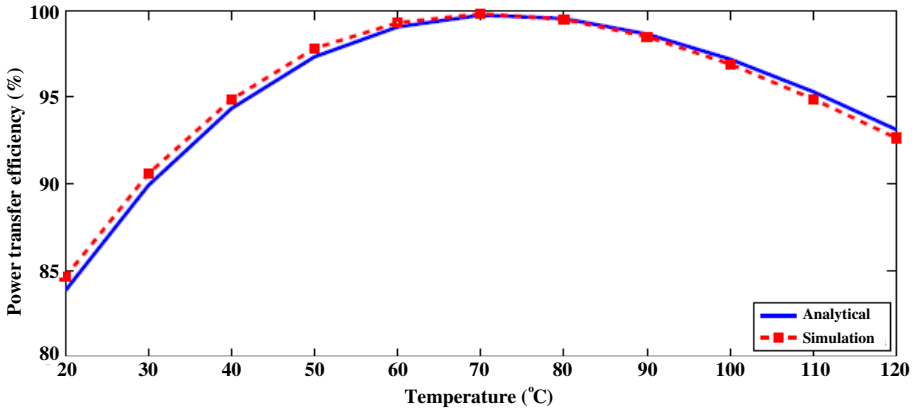

Figure 11. Predicted power transfer efficiency for a 0.03315 N salt water load.

peaks around the optimal load impedance point which corresponds to 70°C. Based on these results an experimental prototype was built.

3. RESULTS AND DISCUSSION

A prototype RF heating applicator was built and tested with salt water loads and samples of WAS. Loads were heated from room temperature to 120°C and the corresponding power transfer efficiencies were calculated to verify the RF heating system design.

3.1. Experimental Test Bed

An experimental test system for heating WAS with a 4.5% solid to liquid mass ratio was implemented. A photo of the test bench is shown Fig. 12. The RF generator consists of a 1 kW class E power amplifier (Directed Energy, Inc, Colorado, model number PRF-1150) which delivers power to heat the load in the applicator. The input signal to the amplifier is a sinewave source generated by an arbitrary waveform generator, Stanford Laboratories model DS345. The power amplifier module requires three external power supplies. Together, the power amplifier, waveform signal generator, and the DC power supplies are integrated to implement the RF generator system shown in Fig. 12.

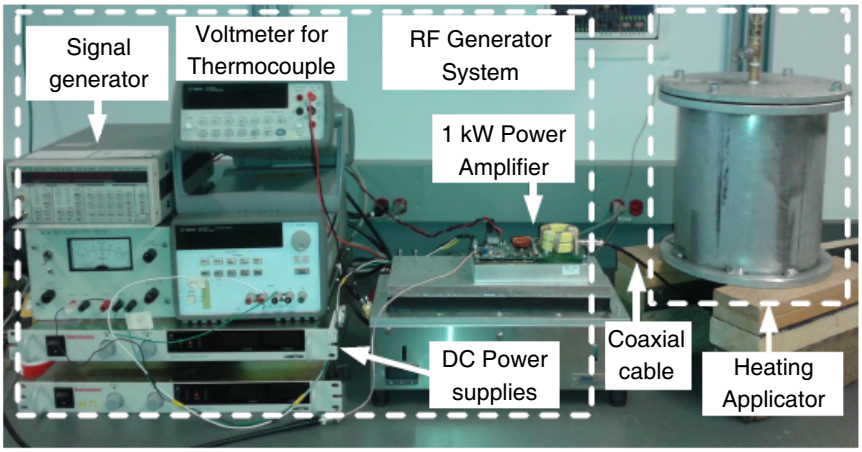

Figure 12. Experimental test bench for the 1 kW RF heating system.

A 30.5 cm length of coaxial cable (RG-58C/U) is used to connect the RF generator to the heating applicator. The equivalent circuit model for the cable, described earlier in Section 2.5.1, was verified experimentally using an Agilent model 5061A vector network analyzer. The measured inductance of the cable is 75 nH and the measured capacitance is 29.2 pF. The corresponding model values were $L_{CC} = 77$ nH and $C_{CC} = 30.8$ pF and the close agreement with experimental measurements supports the choice of the equivalent circuit model topology used for analysis.

The load temperature inside the heating applicator is measured using a digital voltmeter (Agilent 34401A) which measures the potential difference across the leads of the thermocouple. The potential difference is calibrated at room temperature for a K-type thermocouple.

An automated closed loop power control system is implemented using remote instrument control and custom LabView software. Temperature measurements are monitored and the high voltage power supply for the class E power amplifier is controlled to adjust the power delivered to the load. The software implements a control loop that sets the thermal ramp rate which is applied to the load as well as maintains a constant load temperature once the target load temperature is reached.

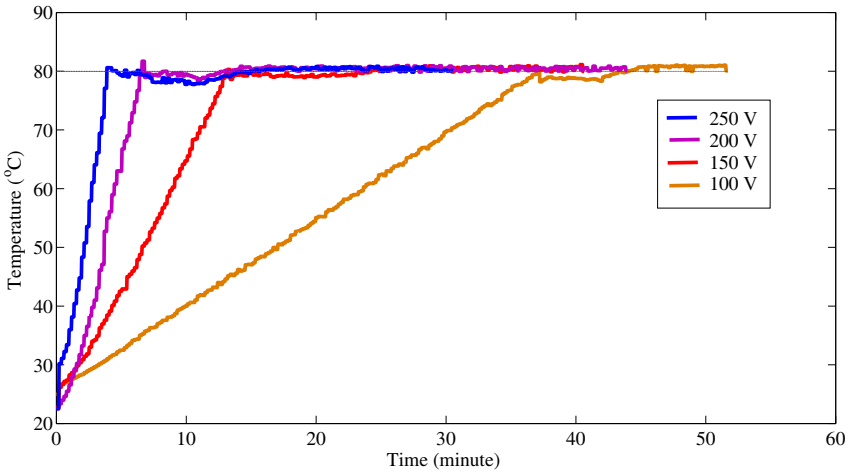

Figure 13. Thermal ramp rate measurements for a salt water load with different power amplifier drain voltages: 250 V (blue line), 200 V (magenta line), 150 V (red line) and 100 V (yellow line).

Table 2. Heating rates for a salt water load (0.03315 N) as a function of the amplifier drain voltage.

Voltage (V)	Time to reach 80°C (min)	Ramp Rate (°C/min)
250	4.2	13.6
200	6.6	8.7
150	10.1	5.7
100	36.7	1.5

3.2. RF Heating System Thermal Profiles

Experiments were made to verify the thermal operation of the RF heating system. The experiments include heating salt water and WAS at different thermal ramp rates and measuring the temperature variation across the load volume.

3.2.1. Thermal Ramp Rate for a Salt Water Load

Salt water loads with a molarity of 0.03315 N were heated at different thermal ramp rates up to a target temperature of 80°C. Experimental results are shown in Fig. 13. Different thermal ramp rates are obtained by changing the supply voltage to the amplifier and results are shown for 100 V, 150 V, 200 V and 250 V. From these measurements, the corresponding thermal ramp rate was calculated for each voltage and the results are shown in Table 2. The thermal ramp rates range from 1.5°C per minute for 100 V to 13.6°C for 250 V. The results show that there is good resolution in controlling thermal ramp rates by adjusting the dc drain supply voltage to the power amplifier.

3.2.2. Thermal Ramp Rate for Waste Activated Sludge

Limited samples of WAS were available for testing and, at this point in the research project, testing was conducted for 100 V only. The results for heating 4.5% WAS are shown in Fig. 14. For comparison, the heating for an equivalent salt water load is also shown. The average ramp rate for the sludge is 1.35°C per minute compared to 1.5°C per minute for the equivalent salt water load (see Table 3). Although salt water has similar electrical characteristics compared to sludge, the physical characteristics of sludge and salt water are different. Sludge is heterogeneous and has a complex mixture of solid organic matter (4.5% by mass). Salt water on the other hand is a homogenous liquid free of solids and the thermal characteristics are primarily determined by the properties of water. The measurements show that a slightly lower thermal ramp rate can be expected for the sludge.

Table 3. Comparison of ramp rates for salt water and WAS. The initial load temperature was 23°C and the target temperature was 80°C.

Load	Time to reach 80°C (min)	Ramp rate (°C/min)
0.03315 N salt water	36.7	1.5
4.5% WAS	32.2	1.86

3.2.3. Temperature Profile Across the Load

An important objective was to design a heating system with uniform heating across the load. The electromagnetic simulations of the electric field profile across the load were shown earlier in Section 2.5.2. If there were no thermal losses in the system, a uniform electric field would create uniform heating and the temperature would be constant across the load; however, there are thermal losses in the RF heating system which creates a deviation from a uniform thermal profile. Thermal conduction losses include heat loss through the aluminum electrodes, the Teflon vessel, and the aluminum enclosure.

The thermal profile of the temperature between the electrodes was measured by inserting a mercury thermometer into the load through a small hole in the electrode which is normally used for a connection to the pressure relief valve. The thermometer was inserted into the load at five equally spaced depths. A large number of experiments were run with the salt water load to measure the temperature gradient across the load. Measurements were made at steady state temperatures from 30°C to 90°C in 10°C steps. A thermal settling time of ten minutes was used before each measurement was made. The upper limit of 90°C is the maximum temperature before the volume of the load expands significantly and starts to bubble through the hole in the top electrode. The results for 70°C and 80°C temperature measurement are shown in Fig. 15.

From the experiments, the following observations are made:

(i) The temperature near the top electrode where the temperature sensor is located is close to the target temperature.

(ii) The temperature in the middle of the load is slightly higher than the target temperature.

(iii) The temperature near the bottom electrode is less than the target temperature and the deviation from the target temperature increases as the temperature increases. For a target temperature of 40°C the maximum temperature deviation is $+2/-3$°C and for a target temperature of 90°C the maximum temperature deviation is $+2/-11$°C.

(iv) The thermal gradient near the bottom electrode is confined to a small region of approximately 1 cm.

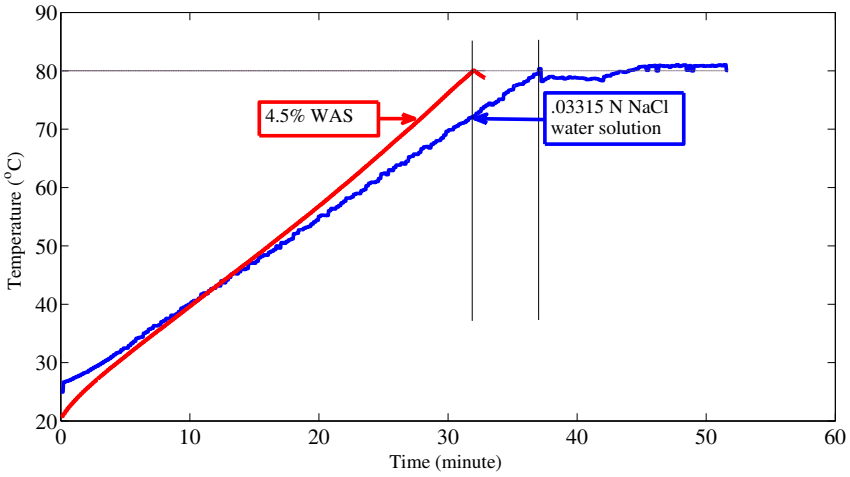

Figure 14. Thermal ramp rate measurement for a 4.5% WAS load with 100 V drain voltage applied to the power amplifier.

As an example, with reference to Fig. 15, for a target temperature of 80°C and with a voltage ramp of 250 V, the temperature varies from 78°C at a distance of 11.3 mm from the bottom electrode to a temperature of 70.8°C at the surface of the bottom electrode. Over the remainder of the load volume, the temperature is within 2°C of the target temperature.

A temperature gradient near the electrodes is expected because of the thermal conduction through the aluminum electrodes. Thermal conduction through the electrodes was considered in the design phase and thin posts are used to connect the electrodes the electrical source. Since the mechanical design of the top and bottom electrodes is similar, a uniform thermal conduction gradient was expected.

Obviously the measurements show an asymmetric thermal gradient near the region of the electrodes, and upon further analysis, the asymmetric gradient can be explained by a change in density as the load is heated. As the load is heated, the density decreases because of the increase in kinetic energy of the molecules in the load. The less dense molecules rise to the top of the Teflon enclosure and gravity acts on the colder molecules that are denser. The movement of mass is a thermal convection process and, in the steady state, the temperature at the bottom of the vessel is cooler than the top of the vessel. Therefore, the primary reason for the steeper temperature gradient at the bottom electrode arises from the orientation of the experimental apparatus where the electrodes are in a vertical profile. Depending on the size of the electrodes, a horizontal profile could reduce temperature variability near the electrodes. Also, thermal insulation in the air space between the teflon load cylinder and the outer housing would minimize thermal losses. These features will be investigated in future work.

3.2.4. Impedance and Power Transfer Measurements

Impedance measurements were made at different temperatures for salt water and WAS loads to verify the design of the RF heating system. The impedance measurements were then used to calculate the power transfer efficiency from the generator to the load using equations shown in Section 2.5.

Impedance measurements for a 0.03315 N salt water load are shown in Fig. 16. For each measurement, the load was heated with a specific thermal ramp rate and held at a steady state temperature for ten minutes. After heating the load to a specific temperature, a vector network analyzer was used to measure the load impedance at the RF connector interface on the heating apparatus. Measurements were made in 10°C steps across the full operating temperature range from 20°C to 120°C. For each temperature measurement point, tests were run with two different thermal ramp rates corresponding to supply voltages of 100 V and 250 V. The thermal ramp rates did not significantly change

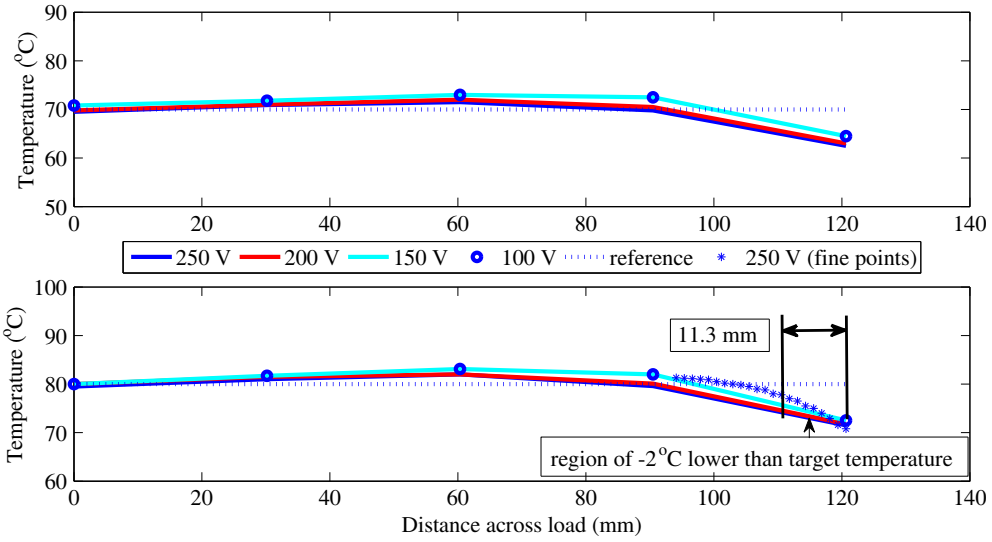

Figure 15. Thermal profile across a 0.03315 N salt water load for a target temperature of 70°C and 80°C with 250 V (blue line), 200 V (red line), 150 V (cyan line), 100 V (blue circle).

the impedance measurements and the results shown in Fig. 16 are the average of the measurements for the 100 V and 250 V thermal ramp rate.

After measuring the impedance characteristics of the salt water load, measurements were made with a 4.5% WAS load. Similar to the salt water load measurements, the WAS load was heated using a 100 V dc voltage thermal ramp and, after reaching the target temperature, the load temperature was maintained for ten minutes before impedance measurements were made. The impedance measurements for WAS are also shown in Fig. 16 and can be compared with the salt water load. The real part of the WAS load impedance is approximately 50 Ω at a temperature of 70°C. The minor differences in the impedance characteristics between WAS and the equivalent salt water load can be attributed to variations in the electrical properties of the sludge.

The impedance measurements shown in Fig. 16 are used to calculate the power transfer efficiency from the RF generator to the load. The results are shown in Fig. 17. For a salt water load, the power transfer efficiency is greater than 93% over a temperature range from 30°C to 120°C. Efficiency peaks between 60°C and 70°C and the peak efficiency point corresponds to the condition where the load impedance is approximately 50 ohms (see Fig. 16). For a WAS load, power transfer efficiency peaks around 70°C, similar to the equivalent salt water load, and efficiency is more than 86% over the entire operating range.

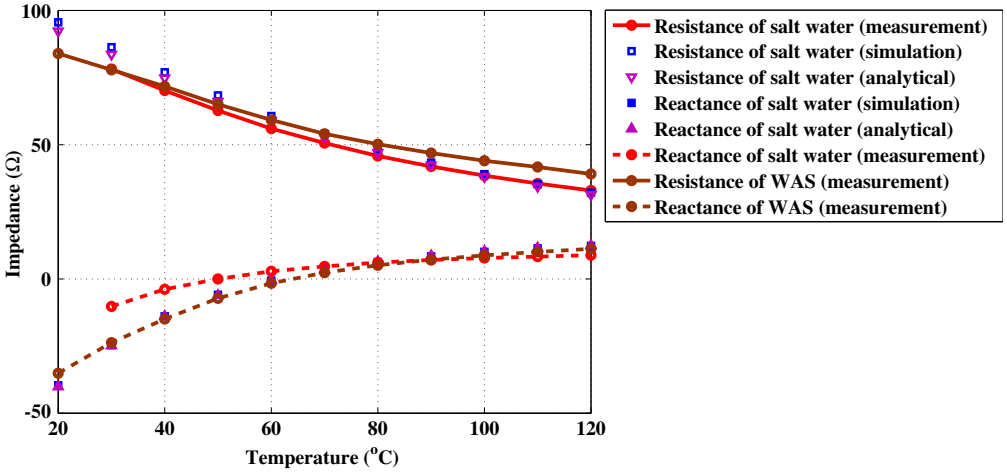

Figure 16. Impedance (resistance and reactance) of salt water and WAS loads as a function of temperature.

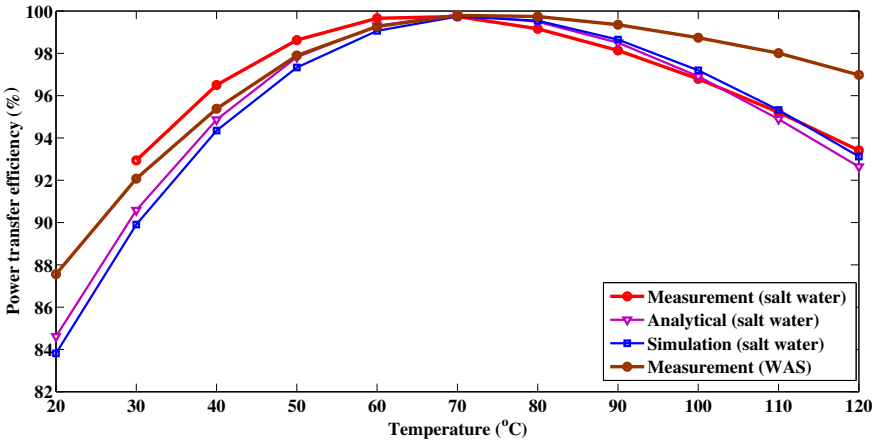

Figure 17. Power transfer efficiency of the RF heating system for salt water and WAS loads.

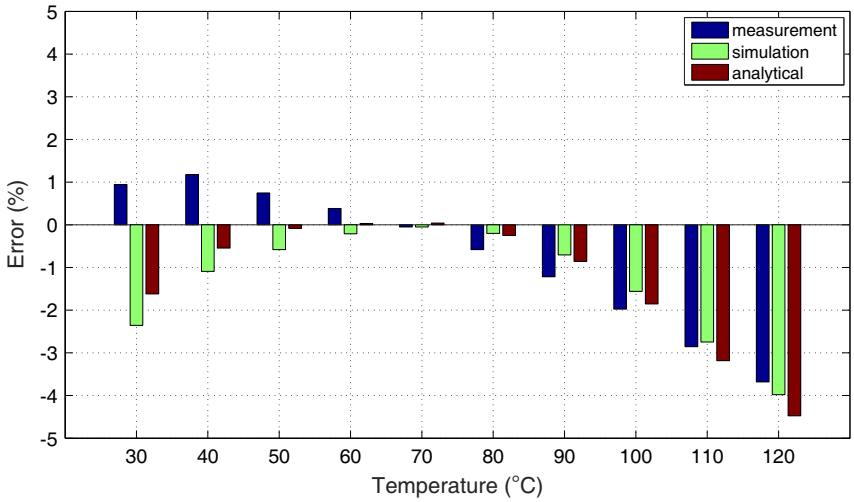

Figure 18. A comparison of the relative error between salt water power transfer efficiency results and the measured results for WAS using data shown in Fig. 17. The corresponding root mean square errors over the 30–120°C temperature range are: 1.69% (using the measured salt water results), 1.76% (using the simulation model results for salt water), and 1.87% (using the analytic model for salt water).

As discussed throughout this paper, an important aspect of the design methodology was to synthesize an equivalent salt water load for analytic, simulation and measurement results. Therefore it is of interest to quantify the differences between the salt water load models and the actual measurements for heating WAS. Using the power transfer efficiency results shown in Fig. 17, the relative errors of the different salt water load models are shown as a function of temperature in Fig. 18. The calibration of the salt water models relative to WAS at a temperature of 70°C is clearly evident and the error is largest at the limits of the temperature range reaching a maximum error of −4.5% at 120°C. The good correlation between the equivalent salt water loads and the actual measured results for heating WAS confirms the hypothesis that WAS can be heated efficiency at a frequency of 13.56 MHz using an ionic heating mechanism.

4. CONCLUSION

This work was motivated by the application of thermal pretreatment for waste activated sludge. Thermal pretreatment processes can improve the biogas yield from anaerobic digesters which are fed with waste activated sludge. Microwave heating has been documented in the literature as a method of heating sludge; however, the penetration of microwave power into the medium limits the volume which can be heated efficiently. Attenuation in the medium also creates non-uniform heating throughout the load.

Based on the dielectric characteristics of WAS, it was hypothesized that more efficient heating could be obtained using RF heating processes at a frequency of 13.56 MHz. At 13.56 MHz, the heating process is created by an ionic conduction current that is activated by the applied RF field and the conduction current is determined by the field strength and the conductivity of the medium. The conduction current leads to uniform heating throughout the entire load volume and therefore overcomes limitations of microwave heating.

A novel coaxial heating applicator with a teflon load cylinder inside a pressure vessel was designed and implemented. Experiments were conducted to evaluate the performance of the RF heating system with both salt water and WAS loads. Impedance measurements were made over a temperature range of 20°C to 120°C and used to calculate the power transfer efficiency of the system. The power transfer efficiency was greater than 86% over the entire temperature range. Overall, the experimental results demonstrate that WAS can be heated efficiently at a frequency of 13.56 MHz and future work is planned to continue investigating RF heating as an energy efficient way to implement thermal pretreatment in anaerobic wastewater processes.

ACKNOWLEDGMENT

The research was financially supported by the National Sciences and Engineering Research Council of Canada (NSERC), Grant Number STPGP 396519-10: "Assessment of biosolids-to-energy options for the Okanagan Valley: a multi-criteria decision making approach."

REFERENCES

1. Braber, K., "Anaerobic digestion of municipal solid waste: A modern waste disposal option on the verge of breakthrough," *Biomass and Bioenergy*, Vol. 9, No. 1, 365–376, 1995.
2. Cakir, F. and M. Stenstrom, "Greenhouse gas production: A comparison between aerobic and anaerobic wastewater treatment technology," *Water Research*, Vol. 39, No. 17, 4197–4203, 2005.
3. Appels, L., J. Baeyens, J. Degrve, and R. Dewil, "Principles and potential of the anaerobic digestion of waste-activated sludge," *Progress in Energy and Combustion Science*, Vol. 34, No. 6, 755–781, 2008.
4. Vlyssides, A. and P. Karlis, "Thermal-alkaline solubilization of waste activated sludge as a pretreatment stage for anaerobic digestion," *Bioresource Technology*, Vol. 91, No. 2, 201–206, 2004.
5. Carballa, M., F. Omil, J. M. Lema, M. Llompart, C. García-Jares, I. Rodríguez, M. Gomez, and T. Ternes, "Behavior of pharmaceuticals, cosmetics and hormones in a sewage treatment plant," *Water Research*, Vol. 38, No. 12, 2918–2926, 2004.
6. Oller, I., S. Malato, and J. Sánchez-Pérez, "Combination of advanced oxidation processes and biological treatments for wastewater decontaminationa review," *Science of the Total Environment*, Vol. 409, No. 20, 4141–4166, 2011.
7. Wei, Y., R. T. V. Houten, A. R. Borger, D. H. Eikelboom, and Y. Fan, "Minimization of excess sludge production for biological wastewater treatment," *Water Research*, Vol. 37, No. 18, 4453–4467, 2003.
8. Bougrier, C., C. Albasi, J.-P. Delgenès, and H. Carrére, "Effect of ultrasonic, thermal and ozone pre-treatments on waste activated sludge solubilisation and anaerobic biodegradability," *Chemical Engineering and Processing: Process Intensification*, Vol. 45, No. 8, 711–718, 2006.
9. Nah, I. W., Y. W. Kang, K.-Y. Hwang, and W.-K. Song, "Mechanical pretreatment of waste activated sludge for anaerobic digestion process," *Water Research*, Vol. 34, No. 8, 2362–2368, 2000.
10. Neyens, E. and J. Baeyens, "A review of thermal sludge pre-treatment processes to improve dewaterability," *Journal of Hazardous Materials*, Vol. 98, No. 1, 51–67, 2003.
11. Eskicioglu, C., K. Kennedy, and R. Droste, "Enhanced disinfection and methane production from sewage sludge by microwave irradiation," *Desalination*, Vol. 248, No. 1, 279–285, 2009.
12. Koupaie, E. H. and C. Eskicioglu, "Below and above boiling point comparison of microwave irradiation and conductive heating for municipal sludge digestion under identical heating/cooling profiles," *Bioresource Technology*, Vol. 187, 235–245, 2015.
13. Saha, M., C. Eskicioglu, and J. Marin, "Microwave, ultrasonic and chemo-mechanical pretreatments for enhancing methane potential of pulp mill wastewater treatment sludge," *Bioresource Technology*, Vol. 102, No. 17, 7815–7826, 2011.
14. Choi, H., S.-W. Jeong, and Y.-J. Chung, "Enhanced anaerobic gas production of waste activated sludge pretreated by pulse power technique," *Bioresource Technology*, Vol. 97, No. 2, 198–203, 2006.
15. Lee, I.-S., P. Parameswaran, J. M. Alder, and B. E. Rittmann, "Feasibility of focused-pulsed treated waste activated sludge as a supplemental electron donor for denitrification," *Water Environment Research*, Vol. 82, No. 12, 2316–2324, 2010.
16. Salerno, M. B., H.-S. Lee, P. Parameswaran, and B. E. Rittmann, "Using a pulsed electric field as a pretreatment for improved biosolids digestion and methanogenesis," *Water Environment Research*, Vol. 81, No. 8, 831–839, 2009.
17. Park, W.-J., J.-H. Ahn, S. Hwang, and C.-K. Lee, "Effect of output power, target temperature, and solid concentration on the solubilization of waste activated sludge using microwave irradiation," *Bioresource Technology*, Vol. 101, No. 1, s13–s16, Jan. 2010.

18. Sólyom, K., R. B. Mato, S. I. Pérez-Elvira, and M. J. Cocero, "The in uence of the energy absorbed from microwave pretreatment on biogas production from secondary wastewater sludge," *Bioresource Technology*, Vol. 102, No. 23, 10 849–10 854, Dec. 2011.
19. Kuglarz, M., D. Karakashev, and I. Angelidaki, "Microwave and thermal pretreatments as methods for increasing the biogas potential of secondary sludge from municipal wastewater treatment plants," *Bioresource Technology*, Vol. 134, 290–297, 2013.
20. Mehdizadeh, S. N., C. Eskicioglu, J. Bobowski, and T. Johnson, "Conductive heating and microwave hydrolysis under identical heating profiles for advanced anaerobic digestion of municipal sludge," *Water Research*, Vol. 47, No. 14, 5040–5051, 2013.
21. Bennamoun, L., Z. Chen, and M. T. Afzal, "Microwave drying of wastewater sludge: Experimental and modeling study," *Drying Technology*, Vol. 34, No. 2, 235–243, 2016, [online], available: http://-dx.doi.org/10.1080/07373937.2015.1040885.
22. Li, Z. Y., R. F. Wang, and T. Kudra, "Uniformity issue in microwave drying," *Drying Technology*, Vol. 29, No. 6, 652–660, 2011.
23. Haque, K. E., "Microwave energy for mineral treatment processes — A brief review," *International Journal of Mineral Processing*, Vol. 57, No. 1, 1–24, 1999.
24. Koupaie, E. H., T. Johnson, and C. Eskicioglu, "Advanced anaerobic digestion of municipal sludge using a novel and energy-efficient radio frequency pretreatment system," *Water Research*, Vol. 118, 70–81, 2017, [online], available: http://www.sciencedirect.com/science/article/pii/S004313541730-2798.
25. Bobowski, J. S., T. Johnson, and C. Eskicioglu, "Permittivity of waste-activated sludge by an open-ended coaxial line," *Progress In Electromagnetics Research Letters*, Vol. 29, 139–149, 2012.
26. Bobowski, J. S. and T. Johnson, "Permittivity measurements of biological samples by an open-ended coaxial line," *Progress In Electromagnetics Research B*, Vol. 40, 159–183, 2012.
27. Stogryn, A., "Equations for calculating the dielectric constant of saline water (correspondence)," *IEEE Trans. on Microwave Theory and Techniques*, Vol. 19, No. 8, 733–736, 1971.
28. "Comsol multiphysics modeling software, version 4.3a," COMSOL Inc.